PNAS RESEARCH ARTICLE | IMMUNOLOGY AND INFLAMMATION OPEN ACCESS

Combined disruption of T cell inflammatory regulators Regnase-1 and Roquin-1 enhances antitumor activity of engineered human T cells

David Mai[a,b], Omar Johnson[b], Jordan Reff[b], Ting-Jia Fan[b], John Scholler[b], Neil C. Sheppard[b,c,1], and Carl H. June[b,c,1]

Contributed by Carl H. June; received November 7, 2022; accepted February 12, 2023; reviewed by Miriam Merad and Kole T. Roybal

A fundamental limitation of T cell therapies in solid tumors is loss of inflammatory effector functions, such as cytokine production and proliferation. Here, we target a regulatory axis of T cell inflammatory responses, Regnase-1 and Roquin-1, to enhance antitumor responses in human T cells engineered with two clinical-stage immune receptors. Building on previous observations of Regnase-1 or Roquin-1 knockout in murine T cells or in human T cells for hematological malignancy models, we found that knockout of either Regnase-1 or Roquin-1 alone enhances antitumor function in solid tumor models, but that knockout of both Regnase-1 and Roquin-1 increases function further than knockout of either regulator alone. Double knockout of Regnase-1 and Roquin-1 increased resting T cell inflammatory activity and led to at least an order of magnitude greater T cell expansion and accumulation in xenograft mouse models, increased cytokine activity, and persistence. However double knockout of Regnase-1 and Roguin-1 also led to a lymphoproliferative syndrome and toxicity in some mice. These results suggest that regulators of immune inflammatory functions may be interesting targets to modulate to improve antitumor responses.

gene editing | inflammation | T cell therapy | solid tumors

Adoptive T cell therapies, in particular chimeric antigen receptor (CAR) T cell therapy, have demonstrated notable efficacy against hematological cancers, leading to U.S. Food and Drug Administration approvals of various CD19 and B cell maturation antigen targeted therapies against B cell malignancies including B-ALL, LBCL, and MM (1–4). Yet, progress toward effective T cell therapies against solid tumors has lagged due to a myriad of factors, a major one being progressive T cell hypofunction against persistent antigen exposure in solid tumors, leading to reduced antitumor effector responses (5, 6). This phenotype, well known as T cell exhaustion, has become recognized as a major challenge to the field, with recent efforts seeking to define, modulate, and ultimately reverse or prevent exhaustion to increase efficacy of T cell therapies in solid tumors (7–10).

A major downstream goal of these important efforts is to rescue effector responses in solid tumor settings. However, specifically enhancing effector functions, such as cytotoxicity, proliferation, and cytokine secretion, can be achieved in various ways, not all of them directly related to exhaustion (11–13). Recent work on intrinsic inflammatory regulators such as Regnase-1 and Roquin-1 in T cells has demonstrated that their disruption can lead to increased antitumor responses (11, 13–15). These proteins act to restrict inflammatory gene expression by targeting the 3'-UTRs of inflammatory gene transcripts leading to degradation, and cause hyperinflammation and autoimmunity when disrupted by loss-of-function mutations (16–19). As a result, we hypothesized that disruption of these genes in engineered T cells could directly increase their inflammatory function and improve their responses in solid tumor settings.

Here, we demonstrate that disruption of both Regnase-1 and Roquin-1 in human engineered T cells increases their antitumor function in solid tumor models in the setting of two clinical-stage immune receptors: the mesothelin-targeting M5 CAR (mesoCAR) and the New York esophageal squamous cell carcinoma 1 (NY-ESO-1)-targeting 8F T cell receptor (TCR) (NYESO TCR). While knockout of either gene alone contributes to distinct phenotypic differences and improves responses in vivo, combined disruption of both genes leads to the greatest antitumor function, with Regnase-1 as the major contributor to the double-knockout profile. These results may inform the design of solid tumor T cell therapies by exploring the multiplex disruption of inflammatory regulators as a general strategy to increase effector functions of engineered CAR and TCR-T cells.

Significance

T cell therapies remain ineffective in solid tumor contexts, which induce hypofunction characterized by reduced cytotoxicity, proliferation, and cytokine function. Recent work has demonstrated that disrupting intrinsic inflammatory regulators, such as Regnase-1, which regulates the stability of inflammatory gene transcripts and induces hyperinflammation when disrupted in T cells, can increase antitumor responses. Here, we validate these observations in two clinical-stage immune receptor models and highlight that additional disruption of Roquin-1, a similar but nonredundant inflammatory regulator, in engineered T cells further improves solid tumor responses, more than disruption of either Regnase-1 or Roquin-1 alone. These results posit immune inflammatory regulators as a promising class of targets for multiplex disruption to develop more potent T cell therapies for solid tumors.

[1]To whom correspondence may be addressed. Email: neil.sheppard@pennmedicine.upenn.edu or cjune@upenn.edu.

This article contains supporting information online at https://www.pnas.org/lookup/suppl/doi:10.1073/pnas.2218632120/-/DCSupplemental.

Published March 15, 2023.

Results

Regnase-1 and Roquin-1 Double Knockout Enhances the Inflammatory Profile of Resting Engineered CAR and TCR-T Cells. To test the hypothesis that we could disrupt immune regulatory proteins Regnase-1 and Roquin-1 to enhance inflammatory function of engineered T cells against solid tumors, we used CRISPR-Cas9 gene editing to knock out Regnase-1 (Reg1-KO), Roquin-1 (Roq1-KO), or both Regnase-1 and Roquin-1 (DKO) in mesoCAR-T cells and TCR-T cells. We screened single-guide RNAs (sgRNAs) against both proteins and identified one top sgRNA each, as determined by % indels, for subsequent use in generating KO cells. KO of Regnase-1 and/or Roquin-1 did not affect the CD3/CD28 bead stimulation-driven expansion kinetics of mesoCAR-T cells or NYESO TCR-T cells during the small-scale manufacturing process, or alter the transduction efficiency, and was achieved with high efficiency (*SI Appendix*, Figs. S1 *A–C* and S2 *A–C*). These findings were anticipated given previous work demonstrating that Regnase-1 and Roquin-1 are specifically targeted for degradation upon TCR stimulation to unleash the production of proinflammatory cytokines, and thus in the short-term both KO and wild-type T cells have reduced Regnase-1 and Roquin-1 activity (20, 21). Flow cytometry characterization of expanded cell products revealed that KO cells displayed an altered baseline activation profile compared with mock cells. Both Reg1-KO and Roq1-KO CD8 T cells expressed elevated levels of CD4, an activation marker on CD8 cells, with DKO cells having the greatest percentage of CD4+ CD8 T cells (Fig. 1*A* and *SI Appendix*, Fig. S3*A*) (22). DKO cells also demonstrated enhanced expression of the costimulatory receptor ICOS but not OX40, both of which are known destabilization targets of Regnase-1 and Roquin-1 (Fig. 1*B* and *SI Appendix*, Figs. S3*B* and S4) (16, 21, 23, 24). While CD69 expression among the different KO and mock CAR-T cells was largely unaltered, CD25 expression was more variable, with Reg1-KO and DKO cells consisting of a larger CD25- subpopulation as well as cells with greater CD25 expression in CD25+ subpopulations of both CD4 and CD8 cells (Fig. 1*C*). Notably, these differences were greater in mesoCAR-T cells than in NYESO TCR-T cells (Fig. 1*C* versus *SI Appendix*, Fig. S3*C*).

Since Regnase-1 and Roquin-1 are both known to regulate a host of inflammatory genes including cytokines, we examined cytokine secretion levels of the cells without exposure to their cognate antigens. DKO cells produced more Th1 and inflammatory cytokines such as IL2, IFNg, TNFa, IL6, and GM-CSF compared to mock cells (Fig. 1*D* and *SI Appendix*, Fig. S3*D*). Interestingly, while DKO cells demonstrated enhanced inflammatory functionality through increased cytokine secretion, greater ICOS expression, and CD4 expression on CD8 cells, they also displayed a greater percentage of central memory T cell subpopulations, which may be due to loss of regulatory effects on notable transcription factor transcripts that are targeted by Regnase-1 (*SI Appendix*, Fig. S5 *A* and *B*) (11, 14). We further profiled these cells transcriptionally by performing bulk RNA sequencing with three donors (two mesoCAR and one NYESO TCR), which agreed with phenotypic data demonstrating enhanced expression of various inflammatory genes. While most of the expression level variation was due to biological differences between donors, among each donor, Reg1-KO and DKO cells clustered together, and distinctly from Roq1-KO and mock cells (*SI Appendix*, Fig. S6*A*). Differential expression analysis between KO groups and mock revealed that DKO cells have the highest number of differentially expressed genes at 79 (59 up, 20 down), particularly up-regulated genes, some of which are known to be related to inflammation including IL17F, IRAK3, IL10, and IL19 (Fig. 1*E*). Compared with mock, Reg1-KO cells had 26 differentially regulated genes (25 up, 1 down) and Roq1-KO cells had only 5 differentially regulated genes (3 up, 2 down), suggesting Reg1-KO is the major driver of the DKO transcriptional phenotype. Transcriptional level expression data of various activation markers (CD40LG, CD44, CD25, and CD69), costimulatory receptor ICOS, and cytokines (IL2, IFNg, and TNFa) aligned with protein-level observations, showing increased levels in Reg1-KO and DKO groups compared to mock, while there were no clear trends among expression of exhaustion markers (PD1, TIM3, LAG3, TIGIT) (Fig. 1*F*). To understand how changes in these genes related to differences in biological pathways, we also performed gene set enrichment analysis of differentially expressed genes, which identified enrichment of the hallmark inflammatory response, interferon gamma response, IL2-STAT5 signaling, IL6-JAK-STAT3 signaling, TNFa signaling via NFkB pathways in Reg1-KO and DKO groups (*SI Appendix*, Fig. S6*B*). These results suggest that DKO of Regnase-1 and Roquin-1, and to some extent KO of Regnase-1 alone enhances the inflammatory potential of resting engineered T cells.

Regnase-1 and Roquin-1 Double Knockout Increases Antitumor Activity. Individual knockout of either Regnase-1 or Roquin-1 in murine T cells and some work in human T cells has been shown to increase antitumor function in models such as the CD19-targeting CAR against B-ALL or OT-I cells against B16 Ova tumors (11, 13, 14). In addition, disrupting the biophysical interaction between Regnase-1 and Roquin-1 alone is sufficient to increase antitumor function in OT-I cells (15). Given the enhanced basal inflammatory profile of DKO T cells and supporting previous studies, we sought to measure their function in solid tumor models using two clinical-stage immune receptors.

To evaluate the in vivo function of KO mesoCAR-T cells, we first utilized a xenograft tumor model in NSG mice. AsPC1 cells, a human pancreatic adenocarcinoma cell line, natively express low levels of mesothelin and were used previously in our lab to establish a model of CAR-T cell dysfunction dependent on chronic antigen exposure (25). AsPC1 cells were subcutaneously implanted on the right flanks of NSG mice and grown until the formation of large established tumors (~250 mm^3) and treatment with a sub-million CAR+ T cell dose (Fig. 2*A*). Under this treatment scheme, mock CAR-T cells performed poorly and did not display significant expansion in vivo, leading to only 1 complete tumor clearance out of 26 mice (3.8%) (Fig. 2 *B* and *D*). In comparison, DKO CAR-T cells were highly effective, leading to complete tumor clearances in over 92% of mice (Fig. 2*B*). Knockout of Regnase-1 or Roquin-1 individually also increased antitumor function, resulting in complete tumor clearances of 85% and 59% respectively (Fig. 2*B*). All KO CAR-T cell groups led to enhanced tumor burden control compared with mock after 4 wk of treatment and showed greater T cell expansion in the peripheral blood (Fig. 2 *C* and *D*). Notably, DKO cells expanded the most with a median on the order of 10^4 T cells/μL blood, several orders of magnitude greater than mock CAR-T cells, followed by Reg1-KO and Roq1-KO with medians on the order of 10^3 and 10^2 T cells/μL blood respectively (Fig. 2*D*). KO cells in the peripheral blood were predominantly CD8+, while less than 20% of mock cells were CD8+ (Fig. 2*E*). Accordingly, all KO CAR-T cells extended survival compared with mock CAR-T cells, with DKO and Roq1-KO CAR-T cells demonstrating the greatest extension in survival at a 0.5×10^6 CAR+ T cell dose (Fig. 2*F*). Mice deaths from the Reg1-KO and DKO treated groups were not due to tumor burden but rather extreme expansion of T cells in the blood. To attempt to mitigate this toxicity, we titrated down the dose of DKO CAR-T cells, finding that by lowering the dose 5-fold and 10-fold, we were able to diminish the extent of expansion and avoid toxicity while still retaining greater antitumor activity than mock CAR-T cells at the original dose (*SI Appendix*, Fig. S17 *A–C*).

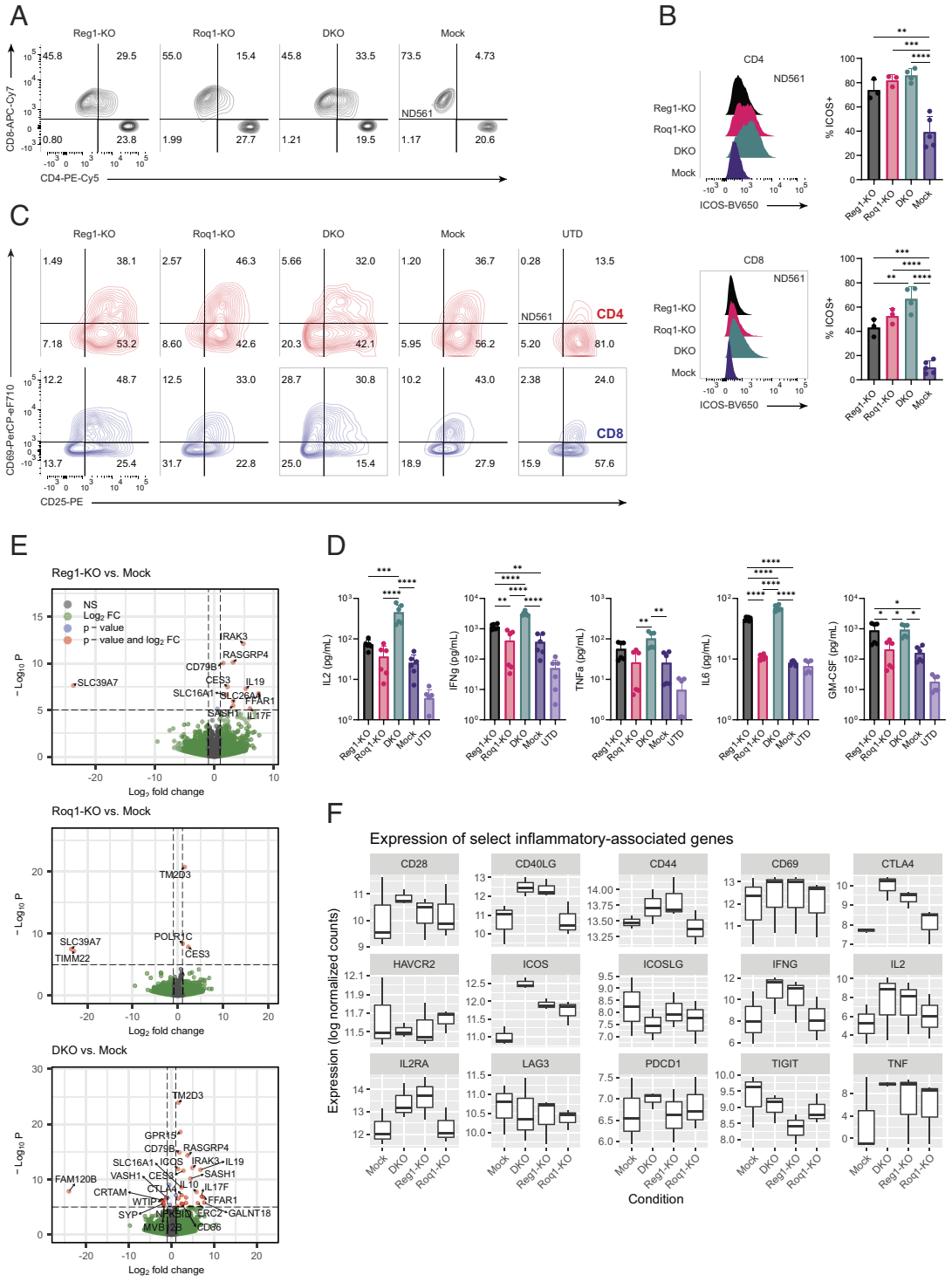

Fig. 1. Regnase-1 and Roquin-1 double knockout alters the activation profile of resting engineered T cells. (*A*) Healthy human donor T cells were subject to CAR-T cell expansion and cryopreserved. Thawed CAR-T cells were rested overnight in media supplemented with cytokines before flow cytometry analysis of CD4 and CD8. Knockout of Regnase-1 and/or Roquin-1 increased expression of CD4, an activation marker, on CD8 T cells. Plots shown are representative of three independent donors. (*B*) Expression of ICOS, a costimulatory receptor, from CAR-T cells rested overnight with cytokines. Left flow plots shown are representative of three independent donors. Right graphs show percentage of ICOS+ T cells summarized among at least three independent donors. *Top* and *Bottom* figures refer to CD4 and CD8 T cells, respectively. Error bars represent SD. One-way ANOVA was used for analysis followed by Tukey's multiple comparisons test. (*C*) Expression of activation markers CD25 and CD69 on CD4 (red) or CD8 (blue) CAR-T cells and UTD controls after coculture with mesothelin-negative K562 cells overnight. Plots shown are representative of two independent experiments from two independent donors each performed in triplicate. (*D*) Secretion of Th1 and inflammatory cytokines (IL2, IFNg, TNFa, IL6, and GM-CSF) measured via Luminex assay. CAR-T cells and untransduced (UTD) T cell controls were cocultured with mesothelin-negative K562 cells overnight, and supernatants were collected for analysis. Data shown are pooled from two independent experiments from two independent donors each performed in triplicate. Error bars represent SD. One-way ANOVA was used for analysis followed by Tukey's multiple comparisons test. (*E*) Volcano plots showing differentially expressed genes between Regnase-1, Roquin-1, and double knockout versus mock engineered T cells (pooled n = 2 CAR-T and n = 1 TCR-T for total n = 3 independent donors) after thaw and overnight rest with cytokines. Genes that are statistically significant (adjusted $P \le 0.005$) and have a Log2FC ≥ 1 are shown in red. Statistical significance was calculated using the Wald test with Benjamini–Hochberg multiple testing correction. (*F*) Expression levels of various inflammatory genes, including Th1 cytokines (IL2, IFNg, TNFa), activation markers (CD25, CD69, CD40LG, PD1, LAG3), and costimulatory receptors (CD28, ICOS). Values shown are log normalized transcript counts of bulk RNA sequencing data from three independent donors (n = 2 CAR-T and n = 1 TCR-T). Box plots show medians, interquartile ranges, minimum, and maximum values. Not shown = not significant, *$P \le 0.05$; **$P \le 0.01$; ***$P \le 0.001$; ****$P \le 0.0001$.

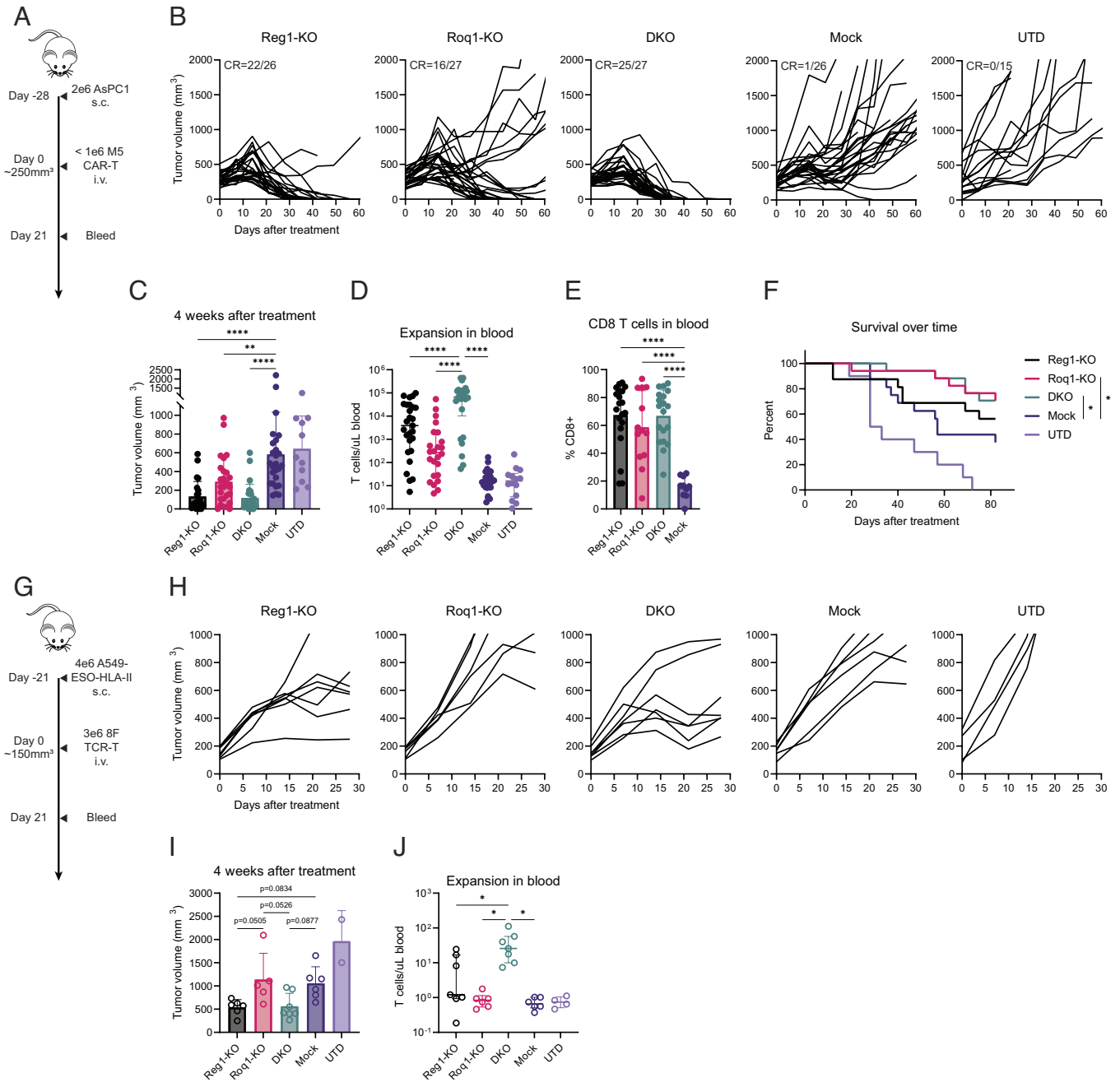

Fig. 2. Regnase-1 and Roquin-1 double knockout increases antitumor function of engineered T cells. (*A*) Schematic of in vivo mouse experiments to evaluate antitumor efficacy of knockout CAR-T cells. A total of 2×10^6 AsPC1 cells were injected subcutaneously on the right flank of NSG mice (n ≥ 15 mice/group across three experiments with two donors). Tumors were grown until sizes reached ~250 mm^3 before treatment with a submillion (0.5×10^6 or 0.75×10^6) dose of mesoCAR+ cells. Mice were monitored, weighed, and measured with calipers once a week, bled after 3 wk, and sacrificed once tumors reached >2 cm in any dimension. Power analysis was not used to determine the sizes of treatment groups. (*B–E*) Antitumor function of Regnase-1 and/or Roquin-1 knockout CAR-T cells compared to mock CAR-T cells with UTD controls. Data shown are pooled from three independent experiments with two independent donors (one donor at 0.5×10^6 mesoCAR+ dose and one donor at both 0.5×10^6 and 0.75×10^6 mesoCAR+ doses). (*B*) Tumor growth over time following treatment with CAR-T cells or UTD control. (*C*) Tumor sizes 4 wk after treatment with CAR-T cells or UTD control. Error bars represent SD. (*D*) Expansion of T cells in peripheral blood 21 d after treatment. Horizontal bars represent median with interquartile ranges. (*E*) CD8 percentage of T cells in peripheral blood 21 d after treatment. Error bars represent SD. For (*C–E*), one-way ANOVA was used for statistical analysis followed by Tukey's multiple comparisons test. (*F*) Kaplan–Meier curve demonstrating that Regnase-1 and/or Roquin-1 knockout CAR-T cells enhance survival compared to mock. Data shown are pooled from two independent experiments with two independent donors at a 0.5×10^6 mesoCAR+ dose (n = 16 Reg1-KO; n = 17 Roq1-KO; n = 17 DKO; n = 16 Mock; n = 10 UTD). Log-rank test was used for statistical analysis. (*G*) Schematic of in vivo mouse experiments to evaluate antitumor efficacy of knockout TCR-T cells. 4×10^6 A549-ESO-HLA-II cells were injected subcutaneously on the right flank of NSG mice. Tumors were grown until sizes reached ~150 mm^3 before treatment with 3×10^6 NYESO TCR+ cells (n ≥ 4 mice/group across two experiments with two donors). Mice were monitored, weighed, and measured with calipers once a week, bled after 3 wk, and sacrificed once tumors reached >2 cm in any dimension. Power analysis was not used to determine the sizes of treatment groups. (*H–J*) Antitumor function of Regnase-1 and/or Roquin-1 knockout TCR-T cells compared with mock TCR-T cells with UTD controls. Data shown are pooled from two independent experiments with two independent donors. (*H*) Tumor growth over time following treatment with TCR-T cells or UTD control. (*I*) Tumor sizes 4 wk after treatment. Error bars represent SD. (*J*) Expansion of T cells in peripheral blood 21 d after treatment. Horizontal bars represent median with interquartile ranges. For (*H*) to (*I*), one-way ANOVA was used for statistical analysis followed by Tukey's multiple comparisons test. Not shown = not significant, $*P \le 0.05$; $**P \le 0.01$; $***P \le 0.001$; $****P \le 0.0001$.

We also evaluated the function of DKO cells in a model of lung cancer using subcutaneous A549-ESO xenografts in NSG mice and the clinical-stage NYESO TCR. Previous reports using similar TCR-T cell models demonstrate some but limited efficacy in preclinical models (26). Here, we established midsized vascularized tumors (~150 mm^3) before treatment with a low dose of 3×10^6 NYESO TCR+ T cells and monitored tumor growth (Fig. 2*G*). In this model, treatment with Reg1-KO and DKO NYESO TCR-T cells displayed the greatest antitumor function and delayed tumor growth compared to mock, while Roq1-KO cells did not (Fig. 2*H*). Accordingly, both Reg1-KO- and DKO-treated groups had the smallest tumors after 4 wk of treatment, while Roq1-KO- and mock-treated groups had comparable tumors that were roughly twice the volume of Reg1-KO- and DKO-treated groups (Fig. 2*I*). Analogous to the results seen with mesoCAR-T cells, DKO NYESO TCR-T cells expanded the most in peripheral blood (Fig. 2*J*). These results demonstrate that DKO of Regnase-1 and Roquin-1 increases antitumor function of CAR and TCR-T cells in solid tumors.

While we observed enhanced antitumor function with single KO and DKO cells in vivo, in vitro functional profiling using short-term assays did not reveal major differences between KO and mock cells. Using freshly thawed and rested T cells, we found that compared with mock, KO cells exhibited similar cytotoxicity and killing, antigen-dependent expression of CD25 and CD69, and proliferation for both CAR-T and TCR-T cells (*SI Appendix*, Figs. S7 and S8). Luminex revealed some increases in Th1 cytokine production induced by receptor-specific antigens, but these differences were minor compared to those at baseline without encountering receptor-specific antigens (Fig. 1*D* versus *SI Appendix*, Figs. S7 and S8).

Regnase-1 and Roquin-1 Double Knockout Cells Retain a Greater Effector Profile. In addition to measuring the antitumor efficacy of KO CAR-T cells, we also used the AsPC1 xenograft model to characterize the profile of tumor infiltrating lymphocytes (TILs). Tumors were grown to the same size as previously described, and mice were treated with 0.5×10^6 CAR+ T cells before harvesting the tumors and spleens at day 14 (Fig. 3*A* and *SI Appendix*, Fig. S15). Consistent with observations seen in the peripheral blood, Reg1-KO and DKO CD4 and CD8 T cells accumulated the most in the tumor, about two orders of magnitude greater than mock CD4 and CD8 T cells, while knockout of Roquin-1 led to a slight increase in tumor infiltration (Fig. 3*B*). Notably, similar numbers of mock cells were found in the tumor compared with UTD cells, suggesting that the mesoCAR alone performs poorly in the context of this tumor model and at this dose (Fig. 3*B*). Compared to mock cells, DKO CD4 and CD8 T cells also accumulated about three orders of magnitude more in the spleen, while single knockout of either Regnase-1 or Roquin-1 led to a more modest increase in accumulation of about 10-fold (Fig. 3*C*). Analogous to accumulation in the tumor, similar numbers of mock T cells were found in the spleen compared with UTD cells (Fig. 3*C*). Flow cytometry analysis of CD4 and CD8 TILs further showed that KO TILs retained higher CAR expression than mock TILs across both CD4 and CD8 populations, most prominently in the Reg1-KO TILs (Fig. 3*D*). Interestingly, while Reg1-KO TILs were least exhausted, as measured by low expression and coexpression of PD1, TIM3, and LAG3, Roq1-KO TILs retained the highest ICOS expression, suggesting that effect of enhanced costimulatory ICOS expression is independent of exhaustion mechanisms (Fig. 3*D*). Reg1-KO and DKO TILs also maintained a greater percentage of central memory T cell subsets, indicative of less terminal differentiation and retention of effector function (Fig. 3*E*).

To further evaluate the functionality of persistent KO cells, we used an in vitro model of serial restimulation to recapitulate the context of extended antigen exposure (Fig. 4*A*). After four stimulations with irradiated K562-Meso, mesoCAR-T cells were assayed for their cytotoxicity and cytokine function. While there were no clear trends in proliferation between KO and Mock CAR-T cells in this restimulation model, DKO CAR-T cells exhibited greater cytotoxicity after serial stimulation (Fig. 4*B*). Intracellular cytokine staining also revealed greater cytokine (IL2, IFNg, TNFa) and effector molecule (CD107a, GrB) functionality in both CD4 and CD8 DKO T cells after serial restimulation (Fig. 4*C*). Specifically, DKO cells were more polyfunctional (IL2+IFNg+TNFa+), expressed more CD107a, GrB, and Ki67 (Fig. 4*C*). We also tested the functional persistence of KO CAR-T cells by performing a tumor rechallenge experiment in mice that demonstrated complete tumor clearance from previous efficacy studies. These mice were rechallenged with 2×10^6 AsPC1 cells on the opposite (left) flank of the original tumor, measured once a week, and bled after 3 wk (Fig. 4*D*). All mice previously treated with KO CAR-T cells demonstrated continued tumor burden control, with near 0mm^3 tumor sizes by day 21, while the mouse previously treated with mock CAR-T cells showed tumor growth kinetics similar to naïve untreated mice controls (Fig. 4 *E* and *F*). Quantification of T cells in the peripheral blood at day 21 after rechallenge revealed enhanced CD4 and CD8 T cell numbers in mice previously treated with KO cells compared with mock cells, with the greatest numbers of T cells observed in mice previously treated with DKO CAR-T cells (Fig. 4 *G* and *H*). Interestingly, enumeration of T cells in the peripheral blood 21 d after primary tumor challenge and 21 d after tumor rechallenge showed that high T cell levels were generally maintained in mice treated with KO cells, especially those treated with Reg-1 KO and DKO CAR-T cells (Fig. 4*I*). Analysis of mice treated with Reg1-KO and Roq1-KO CAR-T cells but not rechallenged demonstrated a more mixed phenomenon with some mice maintaining similar levels to those at 21 d after initial tumor challenge and others showing a large reduction in T cell numbers (*SI Appendix*, Fig. S9). These results suggest that knockout of both Regnase-1 and Roquin-1 contributes to more durable effector function and to enhanced antitumor function in solid tumor models, supporting the hypothesis that combined disruption of these immune regulatory proteins can enhance the function of engineered T cells in solid tumor settings.

Discussion

Here, we bolster prior observations on disrupting negative immune regulators Regnase-1 and Roquin-1 in T cells and build on them by testing individual and dual knockouts of Regnase-1 and Roquin-1 in human T cells engineered with clinical-stage immune receptors against solid tumor antigens. These data add additional contexts in which we see increased antitumor efficacy by knocking out Regnase-1 or Roquin-1 as well as provide results for dual knockout of Regnase-1 and Roquin-1 in solid tumor models leveraging a clinical-stage CAR and TCR in human T cells. Using conventional preclinical methods for producing engineered human T cells, we demonstrated that we could reliably produce CAR-T cells and TCR-T cells with not only single knockouts of Regnase-1 or Roquin-1 but also double knockouts of both genes without noticeable changes in their primary expansion (*SI Appendix*, Figs. S1 and S2). This may be surprising given that Regnase-1 was identified through an in vivo CRISPR screen of metabolic regulators selecting for tumor accumulation and Roquin-1 was identified in a separate CRISPR screen of CD8 T cell fitness genes as a regulator of CD8 T cell expansion in vivo (11, 13). However, the conditions of these in vivo screens differ from those of T cell engineering in vitro, which involves an activation step through CD3/CD28 stimulation that down-regulates endogenous Regnase-1 and Roquin-1 via MALT1-mediated cleavage and proteasomal degradation resulting in a transient protein level "knockout" of Regnase-1 and Roquin-1 (20, 21).

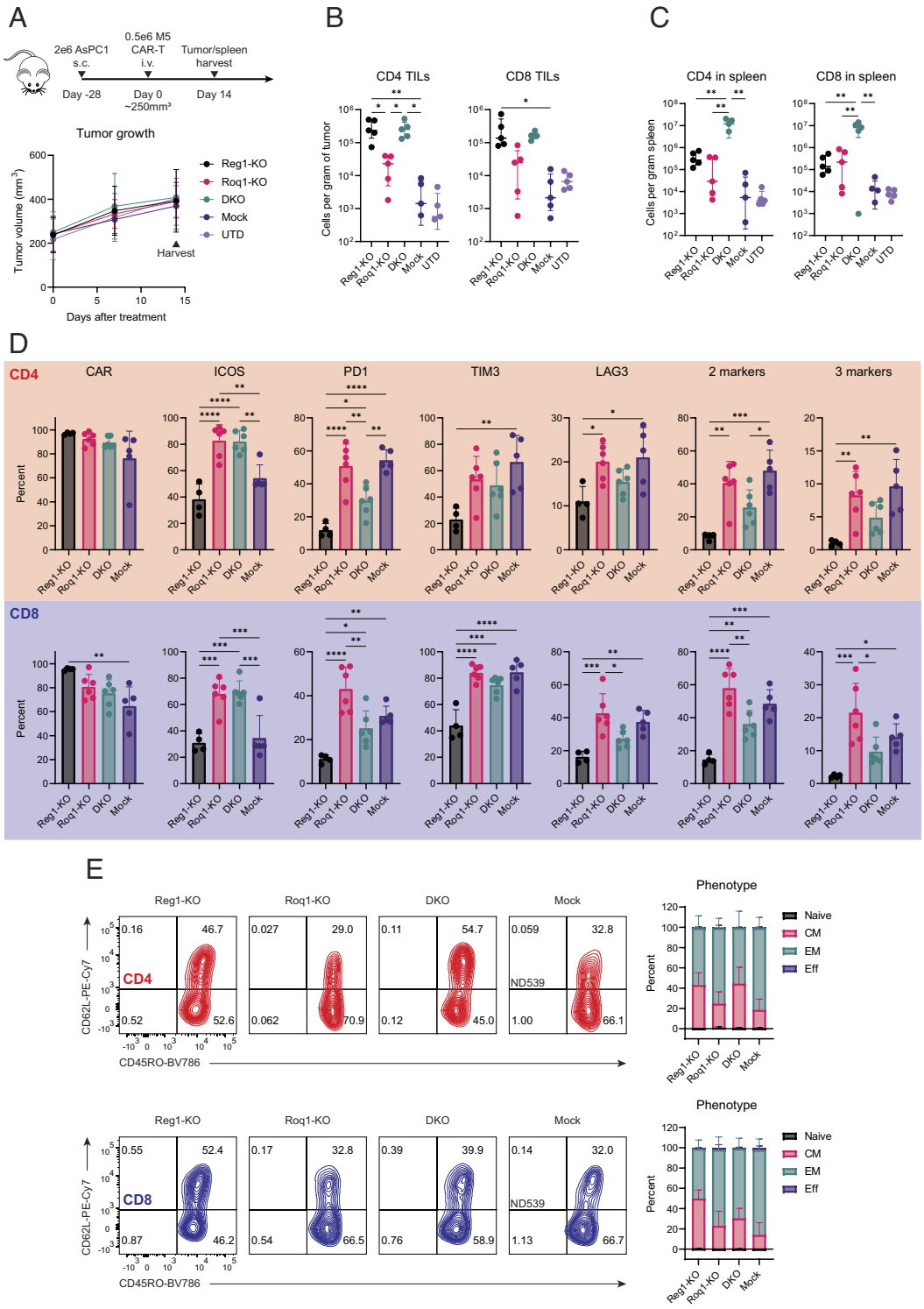

Fig. 3. Regnase-1 knockout enhances in vivo accumulation and functional profile. (*A*) Schematic of in vivo mouse experiments to evaluate distribution of T cells and the phenotype of tumor infiltrating lymphocytes (TILs). A total of 2×10^6 AsPC1 cells were injected subcutaneously on the right flank of NSG mice. Tumors were grown until sizes reached ~250 mm^3 before treatment with 0.5×10^6 mesoCAR+ cells. Mice were monitored, weighed, and measured with calipers once a week for 2 wk, at which point mice were sacrificed and the spleens and tumors were harvested for analysis. (*B–D*) Quantification of TILs and T cells in the spleen 14 d after treatment and phenotyping of TILs. In these figures, one-way ANOVA was used for statistical analysis followed by Tukey's multiple comparisons test. Data shown are representative of three independent experiments in two independent donors (n ≥ 3 per group). (*B*) Quantification of CD4 (*Left*) and CD8 (*Right*) TILs in xenograft tumors. Horizontal bars represent median with interquartile ranges. (*C*) Quantification of the number of CD4 (*Left*) and CD8 (*Right*) T cells in mice spleens. Horizontal bars represent median with interquartile ranges. (*D*) Phenotyping of CD4 (*Top*) and CD8 (*Bottom*) TILs by flow cytometry. Isolated TILs were stained for CAR, ICOS, and exhaustion markers PD1, TIM3, and LAG3, and gated using florescence-minus-one (FMO) controls. Quantification of exhaustion included cells that expressed two markers (sum of percentage of cells that were simultaneously positive for any two of the three exhaustion markers) and three markers (percentage of cells that were simultaneously positive for all three exhaustion markers). Error bars represent SD. (*E*) Quantification of T cell subset distribution for CD4 (*Top*) and CD8 (*Bottom*) TILs. Representative flow plots (*Right*) showing distribution of naïve, central memory, effector memory, and effector T cell subsets as measured by CD45RO and CD62L staining across knockout and mock TILs with summarized graph (*Left*). Data are representative of two independent experiments in two independent donors (n ≥ 3 per group). Error bars represent SD. One-way ANOVA followed by Tukey's multiple comparison test was used for statistical analysis of only the central memory subset data (since all subsets are part of a whole). Not shown = not significant, $*P \le 0.05$; $**P \le 0.01$; $***P \le 0.001$; $****P \le 0.0001$.

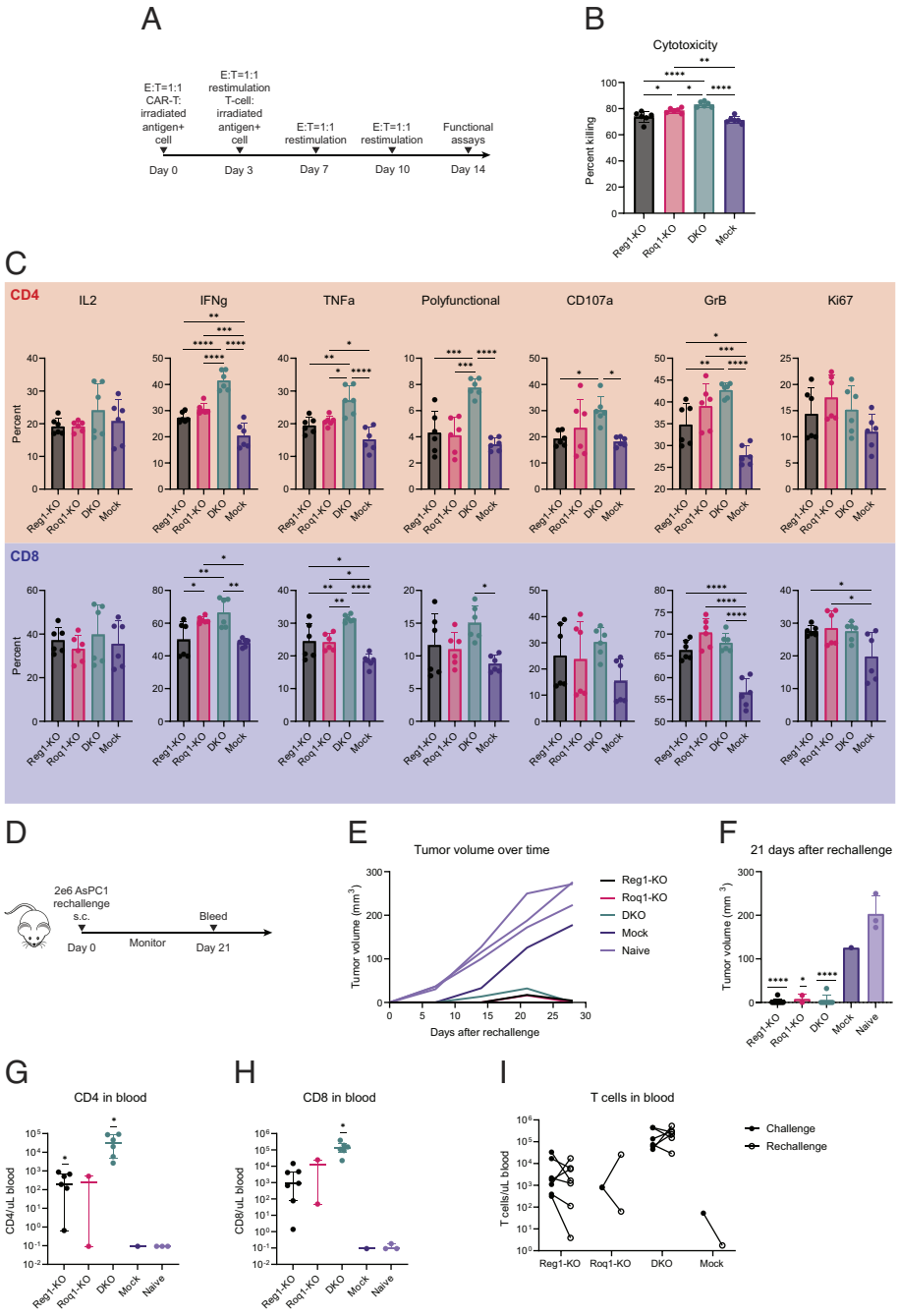

Fig. 4. Regnase-1 and Roquin-1 double knockout enhances functional persistence. (*A*) Schematic of the in vitro restimulation assay to assess functional persistence. mesoCAR-T cells were cocultured with irradiated mesothelin-positive K562 cells at a 1:1 E:T ratio for a total of four stimulations. At each restimulation, T cells were counted by flow cytometry and used to seed the next restimulation at a 1:1 E:T ratio (with respect to total live T cell count, not CAR+ count) in fresh media. Cells were taken for functional assays such as cytotoxicity and intracellular cytokine staining at the fourth stimulation. (*B*) Cytotoxicity of serially restimulated CAR-T cells at various E:T ratios. Data shown are pooled from triplicate experiments with two independent donors. One-way ANOVA followed by Tukey's multiple comparisons test was used for statistical analysis. (*C*) Cytokine expression of serially restimulated CD4 (*Top*) and CD8 (*Bottom*) T cells. T cells were treated with PMA and Ionomycin for an hour before addition of Brefeldin A and Monensin, additional 4-h culture time, and intracellular cytokine staining of Th1 cytokines (IL2, IFNg, TNFa) and degranulation-associated proteins (CD107a, GrB). Polyfunctional indicates simultaneous expression of IL2, IFNg, and TNFa. Data shown are pooled from triplicate experiments with 2 independent donors. (*D*) Schematic of in vivo mouse experiments to evaluate persistence of knockout CAR-T cells and response to tumor rechallenge. Mice that demonstrated a complete response (cleared tumor) from antitumor efficacy studies were used for these experiments. Tumor-free mice were rechallenged with injection of 2×10^6 AsPC1 cells subcutaneously on the opposite (*Left*) flank of the original tumor at least a month after initial tumor clearance. The number of mice per group could not be strictly controlled due to differential responses to initial tumor challenge. Naïve mice that had not been previously challenged with tumor cells were used as controls for tumor growth. Mice were monitored, weighed, and measured with calipers once a week and bled after 21 d. (*E* and *F*) Reponses to tumor rechallenge by knockout and mock CAR-T cells following at least a month from primary tumor clearance. Mice for this experiment (n = 8 Reg1-KO; n = 2 Roq1-KO; n = 7 DKO; n = 1 Mock; n = 3 Naive) were taken from two independent experiments. Power analysis was not used to determine sizes of each group. (*E*) Tumor growth over time after rechallenging previously treated mice with AsPC1 cells. (*F*) Tumor sizes 21 d after rechallenge. One-sample *t* tests were used for pairwise statistical analysis between knockout groups versus mock since the experiment only contained one mock-treated mouse. Error bars represent SD. (*G* and *H*) Quantification of CD4 (*Left*) and CD8 (*Right*) T cells in peripheral blood 21 d following tumor rechallenge. Some data points are not shown due to 0 values on a log-scale plot. Horizontal lines represent median. One-sample *t* tests were used for pairwise statistical analysis between knockout groups versus mock. (*I*) Changes in peripheral T cell numbers between 21 d after initial tumor challenge and 21 d after tumor rechallenge in rechallenged tumor-cleared mice. The number of mice per group could not be strictly controlled due to differential responses to initial tumor challenge. One-way ANOVA followed by Dunnett's multiple comparisons test was used for statistical analysis. Not shown = not significant, $*P \leq 0.05$; $**P \leq 0.01$; $***P \leq 0.001$; $****P \leq 0.0001$.

While primary expansion remained unaffected, baseline rested KO cells displayed an altered inflammatory profile consistent with previous work describing the hyperinflammatory phenotypes of T cells without either Regnase-1 or Roquin-1 (17, 21). These profiles were directly associated with improved antitumor outcomes when testing their function in vivo at a suboptimal therapeutic dose at which unedited mock CAR-T cells or TCR-T cells could not control tumor burden. This was initially surprising because while the KO cells had distinct functional differences at baseline, most notably increased antigen-independent cytokine production, we did not observe any major functional differences during in vitro tumor settings. This may be reminiscent of the phenomenon observed during initial expansion, whereby activation through CD3/CD28 or antigen exposure in an in vitro setting provides sufficient Regnase-1 and Roquin-1 downregulation to obscure any intrinsic short-term benefits.

Analysis in vivo proved to be the illuminating setting that recapitulated the hypothesized outcomes of Regnase-1 or Roquin-1 disruption. Knockout of either Regnase-1 or Roquin-1 alone significantly increased in vivo proliferation in mesoCAR-T cells, and these effects were additive when both genes were knocked out in CAR-T cells and NYESO TCR-T cells. As expected, these effects were correlated with increased accumulation of T cells in both the tumor and the spleen, but also led to splenomegaly in mice treated with DKO cells (*SI Appendix*, Fig. S15*C*). This also contributed to more favorable phenotypic profiles of the T cells in vivo, as the cells encountered less antigen on a per cell basis due to enhanced tumor clearance, potentially allowing cells to retain a less activated and differentiated state with lower expression of canonical exhaustion markers PD1, TIM3, and LAG3. It may be interesting to characterize the function of DKO cells in orthotopic models, to observe whether enhanced accumulation also occurs and drives greater efficacy in a more native tumor environment. Given our results here and previous work showing accumulation of Regnase-1 KO cells in both tumors and normal immune organs such as the spleen, it could be likely that DKO cells similarly demonstrate increased expansion, accumulation, and antitumor responses in orthotopic models.

A notable observation was the maintenance of high levels of T cells in vivo even after tumor burden was completely cleared. This high level of in vivo expansion contributed to some cases of toxicity, especially when mesoCAR-T cells were dosed at higher than 0.5×10^6 cells but could be mitigated with lower doses (*SI Appendix*, Figs. S10 and S17). This toxicity was not mediated through the TCR and was likely not graft-versus-host disease; knockout of the endogenous TCR on mesoCAR-T cells did not rescue toxicity nor significantly change the expansion dynamics in vivo (*SI Appendix*, Figs. S11 *A* and *B* and S12), suggesting that toxicity was more likely attributed to extraordinarily high absolute numbers of T cells per volume blood rather than graft-versus-host effects. KO cells did not expand uncontrollably in IL2-independent culture conditions, suggesting that they do not transform, at least in vitro (*SI Appendix*, Fig. S18). Higher T cell counts in the DKO group corresponded with increased levels of cytokines in the serum, though whether this contributed to toxicity is unclear (*SI Appendix*, Fig. S13). Given toxicity in clinical settings with unedited CAR-T cells, KO CAR-T may have a greater potential for neurotoxicity due to both increased cytokine function and expansion. It will be important for translational efforts to evaluate these safety considerations, which may be done using emerging preclinical safety models (27, 28). In a potential human setting, the expansion of DKO T cells might be limited by competition with normal host T cells that are absent in NSG mice or controlled using a suicide switch such as the iCaspase switch, dasatinib, or a transient strategy for knockdown of Regnase-1 and Roquin-1 (29, 30).

This class of T cell inflammatory regulators present as interesting targets to modulate to enhance T cell therapies. Further work on Regnase-1 and Roquin-1 as well as other regulators of the T cell inflammatory response may reveal other strategies to increase antitumor responses in solid tumor settings. As vital genes in the prevention of hyperinflammatory pathology in endogenous settings, Regnase-1 and Roquin-1 may be interesting candidates not only to explore permanently disrupting, but also transiently disrupting during the manufacturing process or in vivo. Further investigation may provide yet more evidence for modulating the regulatory axis of inflammation as a therapeutic strategy for improving immune cell therapy responses against solid tumors.

Materials and Methods

Primary T Cells and Tumor Cell Lines. Deidentified healthy donor PBMCs were obtained after written informed consent under a University Institutional Review Board-approved protocol and processed to isolate T cells by the Human Immunology Core (HIC) at the Perelman School of Medicine. Cell lines were obtained from the ATCC, ID verified by ATCC human cell line STR profiling, and confirmed negative for mycoplasma using Cambrex MycoAlert mycoplasma detection assay (Promega). AsPC-1 cells were grown in DF20 media consisting of DMEM/F12 (1:1) (Gibco, Life Technologies), 20% fetal bovine serum (Seradigm), and 1% penicillin/streptomycin (Gibco, Life Technologies). K562 and HEK293T cells were cultured in R10 media consisting of RPMI-1640 (Gibco, Life Technologies) with 10% FBS, 10mM HEPES (Gibco), 1% GlutaMAX™ (Gibco), 1 mM Sodium Pyruvate (Gibco), 1% MEM NEAA (Gibco), and 1% penicillin/streptomycin. GFP/CBG-expressing and antigen-expressing (mesothelin, NY-ESO-1) cell lines were generated by lentiviral transduction for cell killing assays.

Lentiviral Vector Production. Lentiviral vector production was performed as previously described (31). Briefly, HEK293T cells were transfected with lentiviral mesoCAR or NYESO TCR and packaging plasmids using Lipofectamine 2000 (Invitrogen) following the manufacturer's protocol. Lentiviral supernatants were collected at 24 and 48 h after transfection and concentrated using high-speed ultracentrifugation. To generate lentiviral stocks, the resulting concentrated lentivirus batches were resuspended in cold R10 media and stored in −80 °C.

CAR-T Cell Production. The anti-mesothelin M5 4-1BB-zeta CAR was previously described (25, 29, 30). CD4 and CD8 T cells were combined at a 1:1 ratio and rested overnight with R10 media supplemented with 5ng/mL human IL7 and 5ng/mL human IL15 (Preprotech). The next day, CRISPR-Cas9 editing was performed, and cells were cultured in cytokine-supplemented R10 media at 5×10^6 cells/mL at 37 °C and activated 4 to 6 h later with Dynabeads® CD3/CD28 CTS™ (Thermofisher) at a 3:1 bead-to-cell ratio at 1×10^6 cells/mL. After 24 h, T cells were transduced at a multiplicity of infection (MOI) of 3. At day 5, beads were removed from cultures. T cell cultures were maintained at 6×10^5 cells/mL. Cell number and volume were monitored daily using Multisizer 3 Coulter Counter (Beckman). Transduced T cells were cryopreserved when they reached a rested state, as determined by cell volume.

TCR-T Cell Production. TCR-T cells were produced similarly to CAR-T cells except for an additional TRAC knockout at the CRISPR-Cas9 editing step and transduction with lentivirus encoding for the NYESO TCR. The NY-ESO-1 targeting 8F TCR was previously described in a clinical trial (32).

CRISPR-Cas9 Editing. Single-guide RNA (sgRNA) sequences targeting Regnase-1 and Roquin-1 were designed using Benchling online software (https://www.benchling.com) and cross-validated with Synthego's guide design verification tool (https://design.synthego.com/#/validate). sgRNA sequences were synthesized by Integrated DNA Technologies (IDT). After screening several (3+) sgRNAs targeting each gene (*SI Appendix*, Table S1), the top sgRNA was selected for downstream experiments. Gene disruption was performed following an optimized protocol previously described (33). Briefly, T cells were washed three times in Opti-MEM™ reduced serum medium (Gibco) and resuspended at 1×10^8 cells/mL in P3 nucleofection solution (Lonza). Ribonucleoprotein (RNP) complexes were generated by incubating each sgRNA (5 μg per 10×10^6 cells) individually with Cas9 nuclease (Aldevron, 10 μg per 10×10^6 cells) for 10 min at room temperature. For no knockout (Mock) groups, no sgRNA was used and for multiple knockout

groups, RNPs targeting each gene were incubated separately before combining. Cells were electroporated in batches of 10×10^6 cells (100 μL) with a mixture of RNP complex and 16.8 pmol of electroporation enhancer (IDT) in electroporation cuvettes (electroporation code EH111) in a 4D-Nucleofector X-Unit (Lonza).

Sequencing. Sanger sequencing of PCR-amplified genomic knockout regions was performed through the DNA Sequencing Facility at the University of Pennsylvania. PCR and sequencing primers are shown in *SI Appendix*, Table S2.

Western blot. Western blotting was used to assess protein level quantification of Regnase-1 and Roquin-1 in T cells. After primary expansion and prior to cryopreservation, 8×10^6 T cells were pelleted and lysed in ice cold RIPA buffer (G Biosciences) supplemented with protease inhibitor (Sigma-Aldrich) for 30 min on ice then centrifuged at 14,000 rpm for 15 min at 4 °C. All lysates were prepared at a concentration of 1×10^6 cells per 10 μL volume of lysis buffer. Whole-cell lysates were boiled for 10 min and then resolved on a 12% Bis-Tris precast gel (Thermofisher). Proteins were transferred onto a polyvinylidene difluoride membrane (Millipore) and then incubated in blocking buffer (LI-COR) for 30 min at room temperature. Primary antibody incubation using rabbit anti-Regnase-1 (Proteintech) or rabbit anti-Roquin-1 (Bethyl Laboratories) and mouse anti-β-actin (Invitrogen) was performed overnight at 4 °C, followed by secondary antibody incubation using IRDye® 800CW goat anti-rabbit IgG (LI-COR) and IRDye® 680RD goat anti-mouse IgG (LI-COR) for 45 min at room temperature.

Flow Cytometry Antibodies. The following antibodies were used (from BioLegend): TCR-Vβ8-PE (clone JR2), CD3-BV711 (clone OKT3), OX40-FITC (clone ATC35), PD1-BV605 (clone NAT105), IL2-APC (clone MQ1-17H12), Ki67-AF488 (clone Ki-67); (from eBioscience): LAG3-APC (clone 3DS223H); (from BD): Streptavidin-PE, CD4-PE-Cy5 (clone RPA-T4), CD8-APC-Cy7 (clone SK1), ICOS-BV650 (clone DX29), TIM3-BV421 (clone 7D3), CD45RO-BV786 (clone UCHL1), CD62L-PE-Cy7 (clone DREG56), CD107a-AF700 (clone H4A3), GrB-CF594 (clone GB11), IFNg-V450 (clone B27), TNFa-PE-Cy7 (clone Mab11), CD25-PE (clone M-A251); (from Jackson Laboratories): Biotin-SP-AffiniPure F(ab')^2 Fragment Goat Anti-Human IgG; (from Invitrogen): CD69-PerCP-eF710 (clone FN50).

Mice. Animal experiments were performed according to protocols approved by the Institutional Animal Care and Use Committee of the University of Pennsylvania. Six-to-eight-wk-old male NOD/scid/IL2rg−/− (NSG) mice were procured from Jackson Laboratories and bred in the vivarium at the University of Pennsylvania and maintained in pathogen-free conditions.

T cell Enumeration. For peripheral blood human T cell counts, submandibular bleeds were performed to collect 50 μL blood for subsequent staining and lysis in Trucount™ tubes (BD). For TIL counts and enumeration of T cells in the spleen, AsPC1 tumors and mice spleens, respectively, were harvested and processed into single-cell suspensions followed by staining and flow cytometry using CountBright™ absolute counting beads (Thermofisher). Gating strategy is shown in *SI Appendix*, Fig. S16. Tumors were dissociated using the human Tumor Dissociation Kit (Miltenyi) according to the manufacturer's protocol, and samples were processed manually through a 70-μm cell strainer (Corning) to obtain a single-cell suspension.

Cytotoxicity Assays. Cytotoxic killing of target cells was assessed using a luminescence-based assay, a real-time impedance-based assay with the xCELLigence Real-Time Cell Analyzer System (ACEA Biosciences), and a real-time imaging-based assay with the Incucyte S3 Live-Cell Analysis System (Sartorius). For luminescence-based assays, T cells were cocultured with luciferase expressing target cells at a range of effector:target (E:T) ratios in flat-bottom 96-well plates for 24 h at 37 °C in R10 media. Target cells include AsPC1 cells and K562-Meso for mesoCAR-T cells or A549-ESO and Nalm6-ESO for NYESO TCR-T cells. After 24 h, living target cells were quantified by the addition of luciferin substrate (GoldBio), and luciferase activity was measured after 10 min using the SpectraMax M3 plate reader (Molecular Devices). The percentage of lysis was determined using the following formula: $1-[\text{Signal}_{\text{sample}}-\text{Signal}_{\text{media only}}]/[\text{Signal}_{\text{tumor only}}-\text{Signal}_{\text{media only}}]$.

Activation Assay. A total of 1×10^5 mesoCAR-T cells or NYESO TCR-T cells were cocultured with K562-Meso or Nalm6-ESO, respectively, overnight in 96-well round-bottom plates in 200 μL R10 media in triplicate. The next day, cells were prepared for flow cytometry staining of CD25 and CD69.

Cytokine Production. Supernatants were sampled from the activation assay (see above) for Luminex multiplex cytokine quantification (MilliporeSigma).

Proliferation Assay. A total of 5×10^4 mesoCAR-T cells or NYESO TCR-T cells were stained with CellTraceViolet dye (Invitrogen) according to the manufacturer's instructions and cocultured with AsPC1 or Nalm6-ESO, respectively, at an E:T ratio of 1:3 in 96-well flat-bottom plates in 200 μL R10 media in triplicate for 1 wk. Wells were topped off with R10 media at the midpoint of the assay to account for volume loss due to evaporation. After 1 wk, cells were assayed via flow cytometry.

Restimulation Assay. A total of 2×10^6 mesoCAR-T cells or NYESO TCR-T cells were cocultured with freshly irradiated K562-Meso or freshly irradiated Nalm6-ESO at an E:T ratio of 1:1 in 6-well plates in 4 mL R10 media in triplicate. At the next stimulation, CD45+ T cells were counted using CountBright Absolute Counting Beads (Invitrogen) by flow cytometry and reseeded with freshly irradiated tumor cells at an E:T ratio of 1:1. T cells and tumor cells in the coculture were both maintained at a concentration of 0.5×10^6 cells/mL. This was repeated for a total of five stimulations before use in functional assays.

Intracellular Cytokine Staining. A total of 4×10^5 T cells were incubated with PMA and ionomycin in 96-well round bottom plates in 200 μL R10 media in triplicate. After 1 h, GolgiPlug™ (BD) and GolgiStop™ (BD) were added to each well, and cells were incubated for an additional 4 h. After a total of 5 h, cells were washed and stained for surface markers for 30 min at 4 °C. Cells were fixed and then permeabilized for intracellular staining of cytokines before flow cytometry.

Bulk RNA-Seq. Total RNA was collected from 2×10^6 T cells with the RNEasy Mini isolation kit (Qiagen). Library preparation and RNA-seq was performed by Novogene on the Illumina NovaSeq 6000 with paired-end 150-bp reads.

IL2-Independent Growth. A total of 2×10^6 T cells were cultured in 2 mL R10 media in 12-well plates and replated in fresh R10 media every 3 to 4 d for 28 d. At each medium change, cells were maintained at a concentration of 1×10^6 cells/mL and counted using the Countess 3 FL Automated Cell Counter (Invitrogen) using Trypan blue (Gibco) as a viability stain. NPM–ALK-transduced T cells were used as a positive control for transformed T cells and have been described previously (34, 35).

Data, Materials, and Software Availability. RNA-seq data will be deposited onto Gene Expression Omnibus (GEO) accession number GSE226522 (36). Code used to process RNA-seq data and generate plots is available on GitHub (https://github.com/davemai/reg1-roq1-knockout) (37). All other study data are included in the article and/or *SI Appendix*.

ACKNOWLEDGMENTS. We thank Regina Young and members of our laboratories for discussions and acknowledge the Human Immunology Core and Stem Cell and Xenograft Core for their assistance. We also thank Jim Riley for a vial of NPM–ALK-transduced T cells as a transformed T cell-positive control. This work was supported by NIH grants 1P01CA214278 and R01CA226983 (C.H.J.), the Parker Institute for Cancer Immunotherapy (C.H.J.), and an Emerson Collective grant 7411021876 (N.C.S.). D.M. is supported by the Fontaine Fellowship, the Norman and Selma Kron Research Fellowship, and the Robert Wood Johnson Foundation Health Policy Research Scholars Program.

Author affiliations: [a]Department of Bioengineering, School of Engineering and Applied Science, University of Pennsylvania, Philadelphia, PA 19104; [b]Center for Cellular Immunotherapies, Perelman School of Medicine, University of Pennsylvania, Philadelphia, PA 19104; and [c]Department of Pathology and Laboratory Medicine, Perelman School of Medicine, University of Pennsylvania, Philadelphia, PA 19104

Author contributions: D.M., N.C.S., and C.H.J. designed research; D.M., O.J., J.R., and T.-J.F. performed research; J.S., N.C.S., and C.H.J. supervised research; D.M. contributed new reagents/analytic tools; D.M. and N.C.S. analyzed data; and D.M., N.C.S., and C.H.J. wrote the paper.

Reviewers: M.M., Icahn School of Medicine at Mount Sinai; and K.T.R., University of California San Francisco Medical Center.

Competing interest statement: The authors have patent filings to disclose, N.C.S. holds equity in Fate Therapeutics, Tmunity Therapeutics, and Pfizer. N.C.S. is a scientific advisor for Immunai and Outpace Bio. C.H.J. has received grant support from Novartis and has patents related to CAR therapy with royalties paid from Novartis to the University of Pennsylvania. C.H.J. is a scientific co-founder and holds equity in Capstan Therapeutics and Tmunity Therapeutics. C.H.J. serves on the board of AC Immune and is a scientific advisor to Alaunos, BluesphereBio, Cabaletta, Carisma, Cartography, Cellares, Cellcarta, Celldex, Danaher, Decheng, ImmuneSensor, Poseida, Verismo, Viracta, and WIRB-Copernicus group. The authors have additional information to disclose. C.H.J. co-published a conference report (https://pubmed.ncbi.nlm.nih.gov/34266886) with Roybal in fulfillment of their shared duties as members of the NCI Cell Therapy Workshop Committee.

1. S. A. Grupp *et al.*, Chimeric antigen receptor-modified T cells for acute lymphoid leukemia. *N. Engl. J. Med.* **368**, 1509–1518 (2013).
2. S. L. Maude *et al.*, Chimeric antigen receptor T cells for sustained remissions in leukemia. *N. Engl. J. Med.* **371**, 1507–1517 (2014).
3. J. N. Kochenderfer *et al.*, Chemotherapy-refractory diffuse large B-cell lymphoma and indolent B-cell malignancies can be effectively treated with autologous T cells expressing an anti-CD19 chimeric antigen receptor. *J. Clin. Oncol.* **33**, 540–549 (2015).
4. N. C. Munshi *et al.*, Idecabtagene Vicleucel in Relapsed and Refractory Multiple Myeloma. *N. Engl. J. Med.* **384**, 705–716 (2021).
5. E. J. Wherry, T cell exhaustion. *Nat. Immunol.* **12**, 492–499 (2011).
6. A. Schietinger *et al.*, Tumor-Specific T Cell Dysfunction Is a Dynamic Antigen-Driven Differentiation Program Initiated Early during Tumorigenesis. *Immunity* **45**, 389–401 (2016).
7. J. Chen *et al.*, NR4A transcription factors limit CAR T cell function in solid tumours. *Nature* **567**, 530–534 (2019).
8. H. Seo *et al.*, BATF and IRF4 cooperate to counter exhaustion in tumor-infiltrating CAR T cells. *Nat. Immunol.* **22**, 983–995 (2021).
9. R. C. Lynn *et al.*, c-Jun overexpression in CAR T cells induces exhaustion resistance. *Nature* **576**, 293–300 (2019).
10. B. Prinzing *et al.*, Deleting DNMT3A in CAR T cells prevents exhaustion and enhances antitumor activity. *Sci. Transl. Med.* **13**, eabh0272 (2021).
11. J. Wei *et al.*, Targeting REGNASE-1 programs long-lived effector T cells for cancer therapy. *Nature* **576**, 471–476 (2019).
12. J. Carnevale *et al.*, RASA2 ablation in T cells boosts antigen sensitivity and long-term function. *Nature* **609**, 174–182 (2022).
13. H. Zhao *et al.*, Genome-wide fitness gene identification reveals Roquin as a potent suppressor of CD8 T cell expansion and anti-tumor immunity. *Cell Rep.* **37**, 110083 (2021).
14. W. Zheng *et al.*, Regnase-1 suppresses TCF-1+ precursor exhausted T-cell formation to limit CAR-T-cell responses against ALL. *Blood* **138**, 122–135 (2021).
15. G. Behrens *et al.*, Disrupting Roquin-1 interaction with Regnase-1 induces autoimmunity and enhances antitumor responses. *Nat. Immunol.* **22**, 1563–1576 (2021).
16. D. Yu *et al.*, Roquin represses autoimmunity by limiting inducible T-cell co-stimulator messenger RNA. *Nature* **450**, 299–303 (2007).
17. S. J. Tavernier *et al.*, A human immune dysregulation syndrome characterized by severe hyperinflammation with a homozygous nonsense Roquin-1 mutation. *Nat. Commun.* **10**, 4779 (2019).
18. K. Matsushita *et al.*, Zc3h12a is an RNase essential for controlling immune responses by regulating mRNA decay. *Nature* **458**, 1185–1190 (2009).
19. P. Anderson, Post-transcriptional regulons coordinate the initiation and resolution of inflammation. *Nat. Rev. Immunol.* **10**, 24–35 (2010).
20. K. M. Jeltsch *et al.*, Cleavage of roquin and regnase-1 by the paracaspase MALT1 releases their cooperatively repressed targets to promote T(H)17 differentiation. *Nat. Immunol.* **15**, 1079–1089 (2014).
21. T. Uehata *et al.*, Malt1-induced cleavage of regnase-1 in CD4(+) helper T cells regulates immune activation. *Cell* **153**, 1036–1049 (2013).
22. Y. B. Sullivan, A. L. Landay, J. A. Zack, S. G. Kitchen, L. Al-Harthi, Upregulation of CD4 on CD8+ T cells: CD4dimCD8bright T cells constitute an activated phenotype of CD8+ T cells. *Immunology* **103**, 270–280 (2001).
23. K. U. Vogel *et al.*, Roquin paralogs 1 and 2 redundantly repress the Icos and Ox40 costimulator mRNAs and control follicular helper T cell differentiation. *Immunity* **38**, 655–668 (2013).
24. E. Glasmacher *et al.*, Roquin binds inducible costimulator mRNA and effectors of mRNA decay to induce microRNA-independent post-transcriptional repression. *Nat. Immunol.* **11**, 725–733 (2010).
25. C. R. Good *et al.*, An NK-like CAR T cell transition in CAR T cell dysfunction. *Cell* **184**, 6081–6100 e6026 (2021).
26. E. K. Moon *et al.*, Blockade of Programmed Death 1 Augments the Ability of Human T Cells Engineered to Target NY-ESO-1 to Control Tumor Growth after Adoptive Transfer. *Clin Cancer Res.* **22**, 436–447 (2016).
27. M. Norelli *et al.*, Monocyte-derived IL-1 and IL-6 are differentially required for cytokine-release syndrome and neurotoxicity due to CAR T cells. *Nat. Med.* **24**, 739–748 (2018).
28. E. Donnadieu *et al.*, Time to evolve: predicting engineered T cell-associated toxicity with next-generation models. *J. Immunother Cancer* **10** (2022).
29. B. S. Jones, L. S. Lamb, F. Goldman, A. Di Stasi, Improving the safety of cell therapy products by suicide gene transfer. *Front. Pharmacol.* **5**, 254 (2014).
30. K. Mestermann *et al.*, The tyrosine kinase inhibitor dasatinib acts as a pharmacologic on/off switch for CAR T cells. *Sci Transl Med* **11** (2019).
31. R. H. Kutner, X. Y. Zhang, J. Reiser, Production, concentration and titration of pseudotyped HIV-1-based lentiviral vectors. *Nat. Protoc.* **4**, 495–505 (2009).
32. E. A. Stadtmauer *et al.*, CRISPR-engineered T cells in patients with refractory cancer. *Science* **367** (2020).
33. S. Agarwal, N. Wellhausen, B. L. Levine, C. H. June, Production of Human CRISPR-Engineered CAR-T Cells. *J. Vis. Exp.* **169**, e62299
34. Q. Zhang *et al.*, The potent oncogene NPM-ALK mediates malignant transformation of normal human CD4(+) T lymphocytes. *Am. J. Pathol.* **183**, 1971–1980 (2013).
35. J. M. Pawlicki *et al.*, NPM-ALK-Induced Reprogramming of Mature TCR-Stimulated T Cells Results in Dedifferentiation and Malignant Transformation. *Cancer Res.* **81**, 3241–3254 (2021).
36. D. Mai *et al.*, Combined disruption of T cell inflammatory regulators Regnase-1 and Roquin-1 enhances antitumor activity of engineered human T cells. *Gene Expression Omnibus (GEO) accession GSE226522*. https://www.ncbi.nlm.nih.gov/geo/query/acc.cgi?&acc=GSE226522. Deposited 2 March 2023.
37. D. Mai *et al.*, Bulk RNAseq analysis of Regnase-1 and/or Roquin-1 knockout primary human T *cells*. davemai/reg1-roq1-knockout. https://github.com/davemai/reg1-roq1-knockout. Deposited 3 March 2023.